Formulation of the moiré patterns formed by superimposing of gratings consisting topological defects: moiré technique as a tool in singular optics detections

2015 J. Opt. 17 105604

(http://iopscience.iop.org/2040-8986/17/10/105604)

IOP Publishing Journal of Optics
J. Opt. 17 (2015) 105604 (11pp) doi:10.1088/2040-8978/17/10/105604

Formulation of the moiré patterns formed by superimposing of gratings consisting topological defects: moiré technique as a tool in singular optics detections

Saifollah Rasouli[1,2] **and Mohammad Yeganeh**[1]

[1] Department of Physics, Institute for Advanced Studies in Basic Sciences (IASBS), Zanjan 45137-66731, Iran
[2] Optics Research Center, Institute for Advanced Studies in Basic Sciences (IASBS), Zanjan 45137-66731, Iran

E-mail: rasouli@iasbs.ac.ir

Received 11 March 2015, revised 22 June 2015
Accepted for publication 29 June 2015
Published 24 August 2015

Abstract

The use of moiré pattern of superimposition of linear forked gratings (LFGs) and Fresnel zone plates (ZPs) has already been reported for study of different physical effects. In spite of a considerable number of applications, there is no comprehensive formulation for this kind of moiré pattern. In this work, we introduce a new family of ZPs containing topological defects that we named defected ZP (DZP) and we present a very simple, uniform, and comprehensive formulation for the moiré pattern of superimposition of two LFGs, two DZPs, and superimposition of an LFG on a DZP, using the reciprocal vector approach. For the case of the two LFGs superimposition, we show that the resulting moiré pattern has a starlike shape or is a large-scale LFG pattern. In the case in which two DZPs are superimposed, we show that the resulting moiré pattern has three general forms: large-scale DZP pattern, starlike pattern, and large-scale LFG pattern. In the superimposition of an LFG on a DZP, in special conditions a new spiral ZP having a topological defect is produced in which its defect number related to the superimposed gratings structures. The presented formulation has potential applications in singular optics measurements.

Keywords: moiré pattern, fringe analysis, forked gratings, Fresnel zone plates, spiral zone plates, topological defects, singular optics

1. Introduction

A moiré pattern is an ancient well-known phenomenon which occurs when two planer periodic or pseudo-periodic structures of equal or nearly equal periods are overlaid. It consists of a new pattern of alternating dark and bright areas with remarkably larger periods which is clearly observed at the superimposition, although it does not appear in any of the original structures [1]. Since 1878, when Lord Rayleigh applied moiré technique to the study of the optical gratings' deformations for the first time, attention to the moiré phenomenon extensively increased and it found numerous applications in different fields such as in metrology and optical testing [1–4]. In recent decades, the moiré technique was used in a wide range of applications in science and technology such as in the measurement of displacements, stresses, vibrations and motions, surface deformations and 3D topography of phase objects [2–5]. In addition, moiré deflectometry is one of the most accurate tools in the measurements of incident wave deflections and wave-front gradients. Recently, it appeared as a powerful tool in the nonlinear refractive index measurement [6, 7], atmospheric turbulence characterization [8–11] as well as in wave-front sensing [12–16]. Furthermore, moiré patterns are demonstrated in quantum imaging on the spatial correlations between entangled photon pairs [17, 18]. Several well-

established approaches have been used for formulation and interpretation of the moiré pattern such as the classical geometric approach [19], parametric equations method [20], and use of Ewald's sphere of reflection [21–24]. The best adapted approach is the spectral approach, which is based on Fourier theory. This approach has been largely developed by Isaac Amidror [1, 25]. New formulations have also been introduced for the interpretation of the moiré patterns based on the spatial averaging and image processing [26, 27]. Presented formulations at most are applicable when a set of periodic or pseudo-periodic functions such as linear, circular, and Fresnel zone plate are considered for the overlaid gratings. In the presence of a phase singularity in the periodic functions of the overlaid gratings such as in the pitch-fork grating or linear forked gratings (LFGs) formulation of the moiré pattern needs modification. It is worth mentioning that, in recent years, moiré patterns featuring superimposition of LFGs and Fresnel zone plates (ZPs) were used for the study of different physical effects [28–34]. Also, moiré patterns of superimposition of spiral zone plates (SZPs) were observed in [35]. In addition, in experimental works they have been used for measurement of the wavefront phase singularity [15, 16]. In another study, formulation of the moiré fringes formed by overlaying two linear gratings with slowly varying parameters is presented [36]. It seems that this technique is going to be an inevitable method in phase singularities measurement [35, 37]. In spite of the considerable number of applications, there is no comprehensive formulation for this kind of moiré pattern. It should be remembered that moiré patterns of superimposition of SZPs were observed by Huguenin *et al* [35]. They have demonstrated the appearance of topological defects in moiré fringes obtained from superposition of two SZPs. We are extending this study to more general patterns, using a reciprocal vector approach. It should be mentioned that we have already used the usual 2D Fourier expansion of the periodic structures [1, 25] and reciprocal vector approach in the analysis of the moiré pattern of moving periodic structures without considering any defects on the structures [38].

In this work, we develop a detailed theoretical description of the different moiré patterns produced by the superimposition of different kinds of gratings containing topological singularities. The topological singularities are naturally described by the azimuthal component of the reciprocal vectors used in the Fourier expansion. It should be mentioned that observation and characterization of this kind of singularities by the Fourier spectral approach has not been reported and it seems that without using a reciprocal approach it is not practicable. In order to present a complete set of moiré patterns illustrating phase singularities, we introduce new sets of ZPs containing topological defects that we named defected ZP (DZP). A simple form of DZP is spiral ZP in which the topological defect is located at the center of the plate. Results of superimposition of two LFGs, two defected ZPs (DZPs), and superimposition of an LFG on a DZP are presented. We simulate different moiré patterns from these structures and offer a detailed discussion based on the presented theoretical tools. For the case of two LFGs superimposition, we show that the resulting moiré pattern has a starlike shape or large-scale LFG pattern. In the case in which two DZPs are superimposed, we show that the resulting moiré pattern has three general forms: large-scale DZP pattern, starlike pattern, and large-scale LFG pattern. In the superimposition of an LFG on a DZP, in special conditions a new spiral ZP having a topological defect is produced in which its defect number is related to the superimposed gratings' structures. Having in mind that in many potential applications of the moiré technique and moiré deflectometry one can use these kinds of gratings instead of the linear gratings, the presented formulation and interpretation for the moiré patterns can be very useful and will find a lot of new applications. As an example, the presented formulation can be used in singular optics measurements because gratings containing topological defects can be produced when a plane wave interferes with a wave containing phase singularity [39, 40].

2. Moiré patterns formulation, reciprocal vector approach

Here, the usual 2D Fourier expansion of the periodic structures [1, 25] is presented. By considering a local spatial frequency for a given periodic structure, its reciprocal vector is determined from the transmission function of the structure. For a superimposition of two periodic structures, the reciprocal vector of the resulted moiré pattern is presented in terms of the reciprocal vectors of the superimposed structures. In the next sections, we will describe the topological singularities of the structures by the azimuthal component of the reciprocal vectors. We show that moiré patterns of static superimposing of different periodic structures possessing topological singularities can be characterized only using the reciprocal vector equation of the resulted moiré patterns. As it was mentioned previously, it seems that without using the reciprocal approach, detection and characterization of this kind of singularities by the Fourier spectral approach is not practicable.

When two gratings with transmission functions $t_1(\boldsymbol{\rho})$ and $t_2(\boldsymbol{\rho})$ are superimposed, transmitted light intensity distribution function will be appear as a multiplication of the transmission functions of the superimposed gratings, $t(\boldsymbol{\rho}) = t_1(\boldsymbol{\rho}) \times t_2(\boldsymbol{\rho})$. One can write the transmission functions of the superimposed gratings as:

$$t_i(\boldsymbol{\rho}) = \sum_{m_i=-\infty}^{\infty} c_{m_i} \exp\left(jm_i \mathbf{G}_i . \boldsymbol{\rho}\right), \qquad i = 1, 2, \qquad (1)$$

where $\boldsymbol{\rho}$ indicates the position vector on the gratings, i shows the number of grating and $\mathbf{G}_i(\boldsymbol{\rho})$ is the reciprocal vector of ith grating in which $\mathbf{G}_i = \frac{2\pi}{\Lambda_i}\hat{G}_i$, where $\hat{G}_i$ is an unit vector perpendicular to the corresponding grating lines and Λ_i is period of the grating. The values of c_{m_i}s are the Fourier series coefficients. Spectrum of the spatial frequencies of $t_i(\boldsymbol{\rho})$ is

given by:

$$T_i(\mathbf{G}) = \sum_{m_i=-\infty}^{\infty} C_{m_i}\delta\big(\mathbf{G} - m_i\mathbf{G}_i\big), \qquad i = 1, 2, \tag{2}$$

where $\delta(\mathbf{G})$ is impulse symbol and C_{m_i} is the amplitude of the corresponding impulse. Based on the convolution theorem, the spectrum of the multiplication of transmission functions of the superimposed gratings can be written as:

$$T(\mathbf{G}) = \sum_{m_{1,2}=-\infty}^{\infty} C_{m_{1,2}}\delta\Big[\mathbf{G} - \big(m_1\mathbf{G}_1 + m_2\mathbf{G}_2\big)\Big], \tag{3}$$

where $C_{m_{1,2}} = C_{m_1} \times C_{m_2}$ [1, 25]. The transmission function in equation (3) has a set of spatial frequencies determined by:

$$\mathbf{G} = m_1\mathbf{G}_1 + m_2\mathbf{G}_2, \qquad m_1, m_2 \in \mathbb{Z}. \tag{4}$$

The first order moiré fringes is determined by plus and minus of minimum of two pairs of frequencies, the vectorial sum and the vectorial difference of $\mathbf{G}_1$ and $\mathbf{G}_2$:

$$\mathbf{G}_{\text{moiré}} = \pm\min\big(\mathbf{G}_1 + \mathbf{G}_2, \mathbf{G}_1 - \mathbf{G}_2\big). \tag{5}$$

Other values of m_1 and m_2 in equation (4) correspond to the higher orders of the moiré patterns. Now, we define a scalar function $g(x, y) = \mathbf{G}(x, y).\boldsymbol{\rho}$ for each of gratings and rewrite the transmittance function of equation (1) for a given grating in the following form:

$$t(x, y) = \sum_{m=-\infty}^{\infty} c_m \exp\left[jmg(x, y)\right]. \tag{6}$$

From the transmission function of the grating, its spatial frequency components are calculated by:

$$\mathbf{G}^{(m)}(x, y) = -j\frac{\nabla t^{(m)}(x, y)}{t^{(m)}(x, y)}, \qquad m = 0, \pm1, \ldots, \tag{7}$$

where m corresponds to the different terms of the transmission function.

Hereafter, for simplicity, we use amplitude gratings with sinusoidal transmission functions. For constructing a sinusoidal grating in equation (6), three terms of $m = 0, \pm1$ are needed. By considering the value of transmission function in a range [0,1], equation (6) for a sinusoidal grating is reduced to [41]:

$$\begin{aligned} t(\boldsymbol{\rho}) &= \frac{1}{2} + \frac{1}{4}\exp[-jg(x, y)] + \frac{1}{4}\exp\left[jg(x, y)\right] \\ &= \frac{1}{2}\{1 + \cos\left[g(x, y)\right]\}. \end{aligned} \tag{8}$$

According to equations (6) and (7), for plus and minus values of m, equal vectors with opposite directions are obtained for $\mathbf{G}$. Therefore, a sinusoidal grating can be defined only by the frequency corresponding to $m = +1$. This means that the local spatial frequency of an amplitude grating with a sinusoidal transmission function in the Cartesian coordinate system is given by [1]:

$$\mathbf{G}(x, y) = \left[\frac{\partial g(x, y)}{\partial x}\hat{x} + \frac{\partial g(x, y)}{\partial y}\hat{y}\right], \tag{9}$$

where $\hat{x}$ and $\hat{y}$ are unit vectors in x and y directions, respectively. When $g(\boldsymbol{\rho})$ is not an explicit function of x and y, equation (9) is used in its general form as:

$$\mathbf{G}(\boldsymbol{\rho}) = \nabla g(\boldsymbol{\rho}). \tag{10}$$

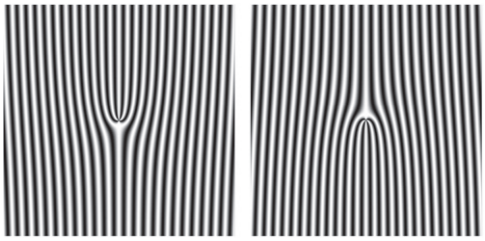

Figure 1. Two typical LFGs with defect numbers of (a) $l = +4$ and (b) $l = -4$. For a size of each of gratings 2.5 × 2.5 cm^2, the period is $\Lambda = 0.1$ cm.

3. Linear forked grating (LFG) presentation

The transmission function of a linear forked grating (LFG) with a sinusoidal amplitude can be written as [42]:

$$t(x, y) = \frac{1}{2}\left[1 + \cos\left(2\pi\frac{x}{\Lambda} - l\varphi\right)\right], \tag{11}$$

where φ denotes the azimuthal angle with respect to the z-axis and Λ is the period of the grating in distances far from the dislocation point located at the center of coordinate system. The value of l is an integer number denoting dislocation of the grating lines that we call it topological defect number or defect number of the grating. Also, we named the dislocation point as a branch point. In figure 1 two typical LFGs with defect numbers of $l = \pm4$ are presented. In this paper we use MATLAB programming for obtaining the simulated images.

For the sinusoidal amplitude LFG, using equations (10) and (11), the reciprocal vector is obtained as:

$$\mathbf{G} = \frac{2\pi}{\Lambda}\hat{x} - \frac{l}{\rho}\hat{\varphi}, \tag{12}$$

where $\hat{x}$ is unit vector along the x-axis and $\hat{\varphi}$ is unit vector of azimuthal angle $\varphi = \tan^{-1}(y/x)$. The radial coordinate from the branch point or center of the coordinate system is given by $\rho = (x^2 + y^2)^{1/2}$.

For general formulation about the moiré patterns of the two LFGs, we need to calculate LFGs' reciprocal vectors, when they are rotated and displaced in their planes. Now, let us apply a rotation by an angle α around the branch point of an LFG and after that apply a displacement to the grating in which its branch point moves from the origin of the

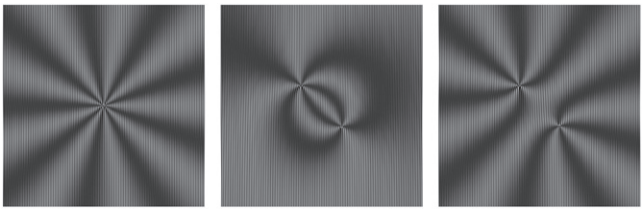

Figure 2. Moiré patterns of superimposition of two LFGs having equal periods of $\Lambda = 0.02$ cm in parallel case: (a) defect numbers are $l_1 = 5$ and $l_2 = -4$ and branch points coincident in common center. (b) gratings separated in two dimensions and $l_1 = 5$ and $l_2 = 4$ (same signs) and (c) $l_1 = 5$ and $l_2 = -4$ (opposite signs).

coordinates system to $(\delta x, \delta y)$. As a result, equation (12) changes to:

$$\mathbf{G}_{\alpha,\delta x,\delta y} = \frac{2\pi}{\Lambda}\left(\cos\alpha\hat{x} + \sin\alpha\,\hat{y}\right) - \frac{l}{\rho_1}\hat{\varphi}_1. \tag{13}$$

Now, at this geometry, coordinates of the branch point are $(\delta x, \delta y)$, $\rho_1 = \left[(x-\delta x)^2 + (y-\delta y)^2\right]^{1/2}$ is radial coordinate from the branch point, and $\hat{\varphi}_1$ is azimuthal unit vector around the branch point. In addition, the azimuthal angle is given by $\varphi_1 = \tan^{-1}[(y-\delta y)/(x-\delta x)] - \alpha$.

4. Moiré patterns of two LFGs

4.1. Moiré patterns of two LFGs in parallel case

We consider superimposition of two LFGs having same periods ($\Lambda_1 = \Lambda_2 = \Lambda$) and different defect numbers ($l_1 \neq l_2$) in a case in which their branch points coincident and are located at the center of the coordinate system. In addition, we assume that the angle between the lines of the superimposed gratings is zero, $\alpha = 0$; we call this case as parallel case. In this case, the reciprocal vector of the resulting moiré pattern using equations (5) and (13) is obtained as:

$$\mathbf{G}_{\text{moiré}} = \frac{l_2 - l_1}{\rho}\hat{\varphi}. \tag{14}$$

This equation indicates that the moiré pattern has a starlike structure. Spatial frequency of the resulted starlike pattern (fringes per length) in azimuthal direction is equal to $f = \frac{|l_2 - l_1|}{2\pi\rho}$ and number of dark or bright radial moiré fringes is $N = 2\pi\rho f = |l_2 - l_1|$. This means that number of moiré fringes is equal to the difference of the gratings' defect numbers. In figure 2(a), a typical moiré pattern of superimposition of two LFGs having $l_1 = 5$ and $l_2 = -4$ is shown, where there are 9 fringes on the moiré pattern.

In second step, we consider that the branch points of the superimposed LFGs are separated and their lines are still parallel, in which case the branch points are moved to $(\mp\frac{\delta x}{2}, \mp\frac{\delta y}{2})$, respectively. In this case, the reciprocal vector of the resulting moiré pattern using equations (5) and (13) is given by:

$$\mathbf{G}_{\text{moiré}} = -\frac{l_1}{\rho_1}\hat{\varphi}_1 + \frac{l_2}{\rho_2}\hat{\varphi}_2, \tag{15}$$

where $\rho_{1,2} = \left[(x \pm \frac{\delta x}{2})^2 + (y \pm \frac{\delta y}{2})^2\right]^{1/2}$ and $\hat{\varphi}_{1,2}$ are unit vectors corresponding to the azimuthal angles defined at the branch points by $\varphi_{1,2} = \tan^{-1}[(y \pm \frac{\delta y}{2})/(x \pm \frac{\delta x}{2})]$. As a simple example, in the superimposition of a linear grating (LG), where its defect number is $l_1 = 0$, on an LFG, the reciprocal vector of the resulted moiré pattern will be equal to $\mathbf{G}_{\text{moiré}} = \frac{l_2}{\rho_2}\hat{\varphi}_2$. This indicates that the produced pattern will be starlike pattern originating from the branch point of the LFG. This kind of moiré pattern has a potential application in the transduction of linear motions into angular velocities.

In figures 2(b) and (c) separating branch points of two LFGs, two sets of starlike moiré patterns appear at the vicinity of branch points. The number of moiré fringes around each branch point is equal to the defect number of the corresponding grating. The moiré pattern at the area far from the branch points has a deformed starlike shape. In figure 2(b), the signs of l_1 and l_2 are same, but for figure 2(c), their signs are opposite. In the area between the branch points, moiré fringes are observed as something like electric field lines of two charges. In spite of the electric field lines of two charges, here, when defect numbers of the gratings have same signs, their fringes is joined together and when the defect numbers have opposite signs, each set of fringes is repelled by other set of fringes.

Now, we derive the above-mentioned properties of the resulting moiré pattern by investigating the phase of the pattern. We consider two LFGs in case $\alpha = 0$, in which their branch points are located at $(\mp\frac{\delta x}{2}, \mp\frac{\delta y}{2})$, respectively. From equation (11) and the fact that the transmission function of the moiré pattern is obtained by multiplying the transmission functions of the gratings, we can deduce the phase distribution of the moiré pattern in following form:

$$\Phi_{\text{moiré}} = \frac{2\pi}{\Lambda}\delta x - \left(l_1\varphi_1 - l_2\varphi_2\right). \tag{16}$$

Now, we calculate the total number of moiré fringes (N) to come out from the branch points. As an integral of moiré pattern phase distribution gradient over a simple closed path encircling branch point(s) is equal to $2\pi N$, we can write

$$N = \left|\frac{1}{2\pi}\oint_C \nabla\Phi_{\text{moiré}}.\,\mathrm{d}\mathbf{s}\right| = \left|\frac{1}{2\pi}\oint_C \mathbf{G}_{\text{moiré}}.\,\mathrm{d}\mathbf{s}\right|, \tag{17}$$

where C is a simple closed integration contour, $\mathrm{d}\mathbf{s}$ is the element of the C contour, and $|\,|$ denotes absolute value. Using equation (16) in equation (17) we have

$$N = \left|-\frac{1}{2\pi}\oint_C \frac{l_1}{\rho_1}\hat{\varphi}_1.\,\mathrm{d}\mathbf{s} + \frac{1}{2\pi}\oint_C \frac{l_2}{\rho_2}\hat{\varphi}_2.\,\mathrm{d}\mathbf{s}\right|. \tag{18}$$

By calculating equation (18) over a circle having a very small radius ρ_1 with center located at the branch point of the first grating, we find $N = |l_1|$, where we use $\rho_1 \ll |\delta x|, |\delta y|$ and $\rho_2 \approx (\delta x^2 + \delta y^2)^{1/2}$. In this case, both integrals in

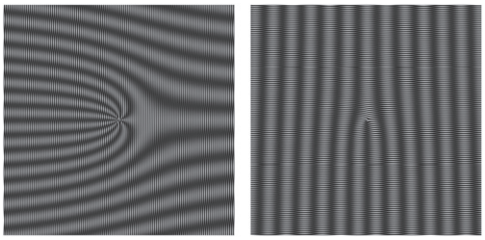

(a) (b)

Figure 3. Typical moiré patterns of two LFGs, here $l_1 = 5$ and $l_2 = -4$ and relative angle of the gratings' lines is: (a) $\alpha \ll 1$ and (b) $\beta \ll 1$. In both cases α and β are positive.

equation (18) are calculated over the first grating's branch point. In addition, for calculating the first integral we use $\mathrm{d}\mathbf{s} = \rho_1 d\varphi_1 \hat{\varphi}_1$. Calculation of the second integral over the first grating's branch point is slightly different. For very small value of ρ_1, values of ρ_2 and $\hat{\varphi}_2$ to be constant and the second term changes to $\frac{l_2}{2\pi\rho_2}\hat{\varphi}_2 \cdot \oint \mathrm{d}\mathbf{s}$. Now, as the closed path integral of $\mathrm{d}\mathbf{s}$ is zero, we consider second integral equal to zero.

Similarly, the number of moiré fringes to come out from branch point of the second grating is determined equal to $|l_2|$. Now, we calculate the path integral over a circle surrounding both of the branch points. It is straightforward to show that the total number of moiré fringes to come out from this circle is equal to $|l_1 - l_2|$. For the same signs of l_1 and l_2, the number of moiré fringes joining the two branch points is equal to the smaller defect number of two gratings. For different signs of l_1 and l_2, the total number of moiré fringes to come out from this circle are equal to $|l_1| + |l_2|$ and consequently there are no joint moiré fringes between the two sets of moiré fringes.

4.2. Rotation effect on moiré patterns of two LFGs

Now, we consider the superimposing of two LFGs having equal periods ($\Lambda_1 = \Lambda_2 = \Lambda$) and different defect numbers ($l_1 \neq l_2$), in which their branch points are coincident and located at the center of the coordinate system ($\rho_1 = \rho_2 = \rho$). We assume that the first grating rotates by $+\frac{\alpha}{2}$ and the other one rotates by $-\frac{\alpha}{2}$ in their planes. In this case, the reciprocal vector of the resulting moiré pattern is calculated from equations (5) and (13):

$$\mathbf{G}_{\text{moiré}} = 2\pi\left(\frac{2\sin\frac{\alpha}{2}}{\Lambda}\right)\hat{y} - \frac{l_1 - l_2}{\rho}\hat{\varphi}. \tag{19}$$

Compared with equation (12) the first term of equation (19) indicates that for small value of the rotation angle, the resulting moiré pattern is a magnified LFG pattern with a period of $\Lambda_{\text{moiré}} = \Lambda/|2\sin\frac{\alpha}{2}|$, in which the direction of the produced moiré fringes is almost perpendicular to the lines of the superimposed gratings. In addition, the defect number of the moiré pattern is equal to the difference of two gratings' defect numbers and its sign is related to their relative rotation angle. By comparing the second terms of the mentioned equations, we see that in a clockwise rotation of the second grating on the first one, the sign of the moiré forked pattern determined by $(l_1 - l_2)$. Comparison between figures 1 and 3(a) shows that for a positive value of l in equation (12), the branching direction of the produced fork-shaped pattern is in the $+\hat{y}$ direction and its reciprocal vector is almost in the x-direction. Similarly, here small values of the rotation angle ($\alpha \ll 1$), the reciprocal vector of produced moiré pattern, are almost in the y-direction and if $(l_1 - l_2)$ is positive, branching of the fork-shaped moiré pattern will be in the $-\hat{x}_0$ direction. A change on the sign of $(l_1 - l_2)$ or α leads to a change on the branching direction of the fork-shaped pattern. In figure 3(a), the moiré pattern of two forked gratings having defect numbers of $l_1 = 5$ and $l_2 = -4$ in which first grating rotated on the second one in trigonometric direction is presented. The number of branches or defect number at the center of the produced forked pattern is equal to 9 and branching is in the $-\hat{x}$ direction.

Now, let us to calculate reciprocal vector of moiré pattern, when two gratings experience a relative rotation angle of close to a straight angle ($\alpha \approx \pi$). We define β as $\alpha = \pi + \beta$, in which $|\beta| \ll 1$. By considering $\cos(\pi/2 \pm \beta/2) = \mp\sin(\beta/2)$ and $\sin(\pi/2 \pm \beta/2) = +\cos(\beta/2)$, and using $\mathbf{G}_1 = \mathbf{G}_{(\pi/2+\beta/2)}$ and $\mathbf{G}_2 = \mathbf{G}_{(-\pi/2-\beta/2)}$, in which we assumed that the first grating rotated by $(\pi + \beta)/2$ and the other one rotated by $-(\pi + \beta)/2$, we can calculate the reciprocal vector of the moiré pattern. By considering both sum and difference terms of $\pm\mathbf{G}_1$ and $\pm\mathbf{G}_2$ and the fact that the frequency of the moiré pattern is the smallest frequency of the superimposition pattern, here equation (5) leads to $\mathbf{G}_{\text{moiré}} = \pm(\mathbf{G}_1 + \mathbf{G}_2)$, then:

$$\mathbf{G}_{\text{moiré}} = 2\pi\left(\frac{2\sin\frac{\beta}{2}}{\Lambda}\right)\hat{x} + \frac{l_1 + l_2}{\rho}\hat{\varphi}. \tag{20}$$

Compared to equations (12) and (20), this equation illustrates a fork-shaped pattern with lines in the y-direction and defect number equal to $|l_1 + l_2|$. Branching of the fork-shaped pattern is in the $-\hat{y}$ direction when values of $(l_1 + l_2)$ and β are positive. Changing the sign of one of these quantities changes the branching direction. This result is presented for the previously mentioned two gratings in figure 3(b) with positive small value of β. In this pattern, the defect number is equal to one and branching is in the $-\hat{y}$ direction.

4.3. Relative displacements of the superimposed gratings

Here, we consider the superimposing of two LFGs having equal periods ($\Lambda_1 = \Lambda_2 = \Lambda$) and different defect numbers ($l_1 \neq l_2$), in which their branch points are separated and located at $\left(\mp\frac{\delta x}{2}, \mp\frac{\delta y}{2}\right)$, respectively. Also, we consider that the gratings are rotated by angles of $\pm\alpha/2$, respectively. The reciprocal vector of the resulted moiré pattern using equations (5) and (13) is given by:

$$\mathbf{G}_{\text{moiré}} = 2\pi\left(\frac{2\sin\frac{\alpha}{2}}{\Lambda}\right)\hat{y} - \left(\frac{l_1}{\rho_1}\hat{\varphi}_1 - \frac{l_2}{\rho_2}\hat{\varphi}_2\right). \tag{21}$$

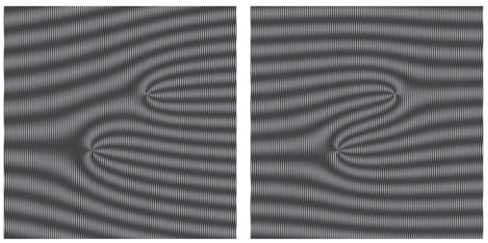

Figure 4. Moiré patterns of two LFGs with size $2.5 \times 2.5\ \text{cm}^2$ in which the second grating with respect to the first one is rotated in the trigonometric direction. Branch points of the first and second gratings are located at $(\mp 0.3, \mp 0.3)$ cm respectively, and (a) $l_1 = 5$ and $l_2 = -4$ (b) $l_1 = 5$ and $l_2 = 4$.

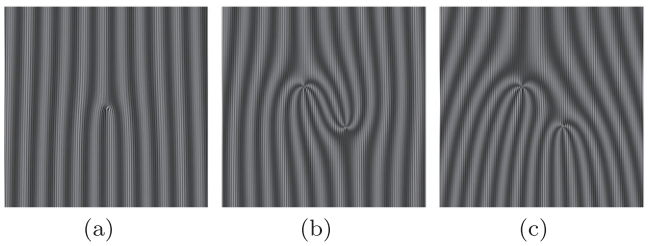

Figure 5. Moiré patterns of superimposition of two LFGs having slightly different periods $\Lambda_1 = 0.02$ cm and $\Lambda_2 = 0.022$ cm in parallel case. In (a) gratings' defect numbers are $l_1 = 5$, $l_2 = 4$ and their branch points coincident. In (b) and (c), gratings' branch points are separated and defect numbers are $l_1 = 5$, $l_2 = 4$, and $l_1 = 5$, $l_2 = -4$, respectively.

This relation indicates two different magnified fork-shaped patterns with centers located at $\left(-\frac{\delta x}{2}, -\frac{\delta y}{2}\right)$ and $\left(\frac{\delta x}{2}, \frac{\delta y}{2}\right)$, respectively. At the area far from the branch points of the gratings, the pattern is a set of almost parallel lines in the x-direction. The defect number of the produced pattern around location $\left(-\frac{\delta x}{2}, -\frac{\delta y}{2}\right)$ is l_1 and for the other one which is placed at $\left(\frac{\delta x}{2}, \frac{\delta y}{2}\right)$ is $-l_2$. Branching direction of the produced fork-shaped moiré patterns depends on the sign of relative angle and their defect numbers. For positive value of α, directions of the produced fork-shaped patterns are determined by the signs of the defect numbers. Both the positive sign of l_1 and negative sign of l_2 are corresponding branching directions in the $+\hat{x}$ direction and for the opposite sign of each one, it changes to $-\hat{x}$ direction. As an example, in figures 4(a) and (b) moiré patterns of two gratings with the same signs and different signs of the defect numbers are shown, respectively. For $\alpha = 0$, the shape of the produced moiré pattern changes to the parallel case which was discussed previously.

4.4. Moiré patterns of two LFGs having slightly different periods in parallel case

In the superimposition of two LFGs having slightly different periods, in the parallel case, from equation (12) reciprocal vector of the produced moiré pattern is given by:

$$\mathbf{G}_{\text{moiré}} = \left(\frac{2\pi}{\Lambda_1} - \frac{2\pi}{\Lambda_2}\right)\hat{x} - \left(\frac{l_1}{\rho_1}\hat{\varphi}_1 - \frac{l_2}{\rho_2}\hat{\varphi}_2\right), \tag{22}$$

where $\hat{\varphi}_{1,2}$ are unit vectors of azimuthal coordinates $\varphi_{1,2}$ defined at the corresponding branch points, and $\rho_{1,2}$ are the radial coordinates measured from the corresponding branch points. The resulting moiré pattern is a magnified fork-shaped pattern in which moiré fringes at the area far from the branch points are almost in the y-direction and their spacing is $\Lambda_{\text{moiré}} = (\Lambda_1\Lambda_2)/|\Lambda_1 - \Lambda_2|$. Branching of the moiré fringes occurs on the branch point(s) of the superimposed gratings. In figure 5 different moiré patterns of two LFGs having slightly different periods in parallel case are presented.

5. Presentation of Fresnel ZPs containing topological defects

A zone plate consists of a set of radially symmetric rings, known the Fresnel zones, which alternate between opaque and transparent. These zones switch at radii where defined by [43]:

$$\rho_n^2 \approx n\lambda f_1 = ns, \tag{23}$$

where n is an integer number indicates the number of rings and f_1 is the first focal length for an incident plane wave with wavelength of λ when the ZP is used as a diffractive lens. We call $s = \lambda f_1$ as the ZP constant. The transmittance function of a ZP can be expressed in a Fourier series as:

$$t(\rho) = \sum_{m=-\infty}^{\infty} a_m \exp\left(\frac{jm\pi\rho^2}{s}\right), \tag{24}$$

where $\rho = \left(x^2 + y^2\right)^{1/2}$ and a_ms are expansion coefficients. Similar to the linear gratings, as discussed before, by considering the terms correspond to $m = 0, \pm 1$ in the expansion, generates sinusoidal ZP function. By use of equation (10), reciprocal vector of the resulting grating contains plus and minus of:

$$\mathbf{G} = \frac{2\pi\rho}{s}\hat{\rho}, \tag{25}$$

which $\hat{\rho}$ is the unit vector corresponding to radial coordinate. Spatial period at a given point defined as:

$$\Lambda(\rho) = \frac{s}{\rho}, \tag{26}$$

where it depends on ρ. A typical sinusoidal amplitude Fresnel ZP is shown in figure 6(a).

5.1. Presentation of ZPs containing topological defects

By adding an additional term to the phase of a ZP, which depends on the azimuthal coordinate, we can introduce a

Figure 6. (a) A typical sinusoidal ZP with ZP constant of $s = 0.1$ cm^2, (b) A typical SZP with same constant and defect number of $l = 3$, and (c) A typical DZP with same s and l in which branch point's coordinates are $(x_0, y_0) = (0.6, 0.6)$ cm. Size of all gratings are 2.5×2.5 cm^2.

ZP containing a topological defect. The center of the azimuthal angle coordinate system may be coincident with the center of the ZP coordinate system or not. Transmission function of this kind of ZPs with a sinusoidal amplitude is given by:

$$t(\boldsymbol{\rho}) = \frac{1}{2}\left[1 + \cos\left(\frac{\pi\rho^2}{s} - l\varphi'\right)\right], \tag{27}$$

where φ' is the azimuthal angle defined at the branch point and we have:

$$\varphi' = \tan^{-1}\left(\frac{y - y_0}{x - x_0}\right), \qquad \rho = \left(x^2 + y^2\right)^{\frac{1}{2}}, \tag{28}$$

where (x_0, y_0) are the branch point's coordinates in the ZP coordinate system. We named this kind of ZPs that contain topological defects DZPs. When the branch point lies at the center of a ZP, it named as spiral ZP (SZP). Figure 6(b) shows a typical SZP pattern having a defect number equal to 3. In figure 6(c) a DZP having a branch point apart from the center of the ZP is shown. For positive value of defect number, branching direction will be in the azimuthal unit vector direction. Reciprocal vector of the grating using equation (10) is given by:

$$\mathbf{G} = \frac{2\pi\rho}{s}\hat{\rho} - \frac{l}{\rho'}\hat{\varphi}', \tag{29}$$

where $\hat{\varphi}'$ is unit vector corresponding to the azimuthal coordinate φ' defined from the branch point and $\rho' = [(x - x_0)^2 + (y - y_0)^2]^{1/2}$.

Fourier spectrum analysis of SZP already is used in signal processing [44]; as a potential application, it can be extended to DZPs.

6. Moiré patterns of two DZPs

In the following, we investigate several cases for superimposition of two DZPs. In a general case, we assume that the centers of DZPs (not the locations of the branch points) coincident together and the corresponding branch points located at $\left(x_{0_1}, y_{0_1}\right)$ and $\left(x_{0_2}, y_{0_2}\right)$, respectively. Also,

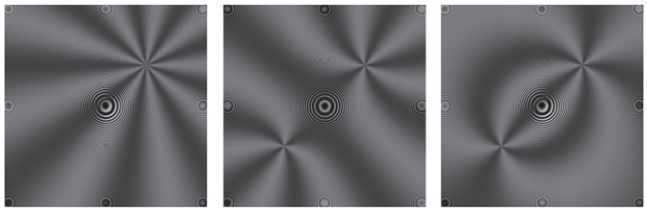

Figure 7. Different typical moiré patterns of superimposition of two DZPs with same ZP constants ($s = 0.006$ cm^2). In (a) defect numbers of the gratings are $l_1 = 5$ and $l_2 = -4$ and branch points coincident at coordinates $(x_0, y_0) = (0.5, 0.5)$cm. In (b) defect numbers are not changed, but the branch point of the second grating moved to $(-0.5, -0.5)$cm. In (c) the value of l_2 changed to +4.

we assume that the defect numbers and the ZPs' constants are not identical, $l_1 \neq l_2$ and $s_1 \neq s_2$. In this case, using equations (5) and (29) reciprocal vector of the moiré pattern obtained as:

$$\mathbf{G}_{\text{moiré}} = 2\pi\rho\left(\frac{1}{s_2} - \frac{1}{s_1}\right)\hat{\rho} - \left(\frac{l_2}{\rho'_2}\hat{\varphi}'_2 - \frac{l_1}{\rho'_1}\hat{\varphi}'_1\right), \tag{30}$$

where $\hat{\varphi}'_{1,2}$ are unit vectors of the azimuthal coordinates $\varphi'_{1,2}$ defined at the corresponding branch points, and $\rho'_{1,2}$ are radial coordinates measured from the same points.

In a special case, in which the branch points of two gratings coincident, $\left(x_{0_1}, y_{0_1}\right) = \left(x_{0_2}, y_{0_2}\right) = (x_0, y_0)$, and gratings' constants are equal, $s_1 = s_2$, it is easy to show that resulting moiré pattern has a starlike shape and has a number of moiré fringes equal to $|l_2 - l_1|$. By substituting $\hat{\varphi}'_1 = \hat{\varphi}'_2 = \hat{\varphi}'$ and $\rho'_1 = \rho'_2 = \rho'$ in equation (30) we have:

$$\mathbf{G}_{\text{moiré}} = \frac{l_2 - l_1}{\rho'}\hat{\varphi}', \tag{31}$$

where it is similar to equation (14), with the exception that here starlike shape centered at (x_0, y_0) instead of common centers of the gratings (see figure 7(a)).

In a case where branch points of the gratings not coincident, using equation (17) one can show that the resulting moiré patterns will be similar to the moiré patterns of the two LFGs superimposition in the parallel case discussed before. The results are shown in figures 7(b) and (c) for the opposite and same signs of l_1 and l_2, respectively.

Now, we consider that the gratings' constants are not identical. According to equation (30), the resulting pattern is a DZP shape pattern with a new ZP constant of $s = s_1 s_2 / |s_1 - s_2|$. Here we call the resulting ZP's constant moiré fringes spacing. When the branch points of the superimposed DZPs coincident, the resulting pattern is a magnified DZP having a branch point placed on the gratings' branch points. In this case we have:

$$\mathbf{G}_{\text{moiré}} = 2\pi\rho\left(\frac{1}{s_1} - \frac{1}{s_2}\right)\hat{\rho} - \frac{l_1 - l_2}{\rho'}\hat{\varphi}'. \tag{32}$$

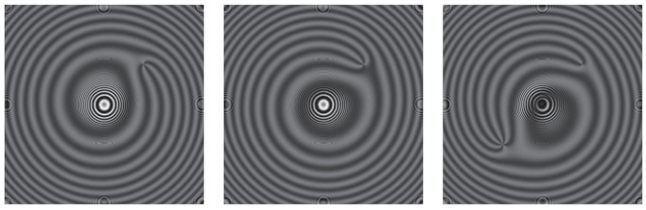

Figure 8. Typical moiré patterns of two DZPs having $l_1 = 2$ and $l_2 = 5$. In (a) $s_1 = 0.006\ \text{cm}^2$, $s_2 = 0.0063\ \text{cm}^2$, and branch points coincident and located at $(x_0, y_0) = (0.5, 0.5)$ cm. In (b) s_1 and s_2 take each others values are given in (a). In (c) branch points are separated from each other in which $(x_{0_1}, y_{0_1}) = (0.5, 0.5)$cm and $(x_{0_2}, y_{0_2}) = (-0.5, -0.5)$ cm.

The number of moiré fringes comes out from branch point, is equal to the difference of the defect numbers $|l_1 - l_2|$. For $s_2 > s_1$, by comparing equations (32) and (29), we see that branching direction is determined by sign of $(l_1 - l_2)$ and for $s_1 > s_2$, this direction is changed. These behaviors are illustrated in figures 8(a) and (b).

Now, let us assume that the branch points are apart from each other. In this case, according to equation (30), the resulting moiré pattern will have two branch points appearing on the branch points of the gratings. The defect number at each branch point is equal to the defect number of the corresponding grating. When $s_2 > s_1$, the branching direction corresponding to the first grating is the same as the sign of l_1, and the direction of the second branching obeys the sign of $-l_2$. This behavior changes when $s_1 > s_2$ as shown in figure 8(c).

6.1. Relative displacements of the superimposed gratings

In the superimposition of two ZPs, in which their centers separated from each other, the produced moiré fringes are a pattern of parallel fringes. In this case, moiré fringes' spatial period is related to distance of the centers of the ZPs and the direction of the moiré fringes is perpendicular to the displacement direction [28]. Here, again we consider a same coordinate system for both of ZPs, in which ZPs' centers are symmetrically separated at the selected coordinate system. Now, we need to find a modified reciprocal vector formula for a DZP, when its center is not coincident with the origin of the coordinate system. We consider a DZP, in which its center's coordinates change from origin (0, 0) to $\left(\frac{\delta x}{2}, \frac{\delta y}{2}\right)$. In this case, coordinates of the branch point of the DZP will change from (x_0, y_0) to $\left(x_0 + \frac{\delta x}{2}, y_0 + \frac{\delta y}{2}\right)$ and the reciprocal vector in equation (29) for this grating should be modify to the following form:

$$\mathbf{G}_{\frac{\delta x}{2},\frac{\delta y}{2}} = \frac{2\pi\rho_1}{s}\hat{\rho}_1 - \frac{l}{\rho'_1}\hat{\varphi}'_1, \tag{33}$$

where, the parameters ρ_1, ρ'_1 and unit vectors $\hat{\rho}_1$ and $\hat{\varphi}'_1$ defined as below:

$$\rho_1 = \left[\left(x - \frac{\delta x}{2}\right)^2 + \left(y - \frac{\delta y}{2}\right)^2\right]^{\frac{1}{2}},$$

$$\rho'_1 = \left[\left(x - x_0 - \frac{\delta x}{2}\right)^2 + \left(y - y_0 - \frac{\delta y}{2}\right)^2\right]^{\frac{1}{2}},$$

$$\hat{\rho}_1 = \frac{1}{\rho_1} \times \left[\left(x - \frac{\delta x}{2}\right)\hat{x} + \left(y - \frac{\delta y}{2}\right)\hat{y}\right],$$

and

$$\hat{\varphi}'_1 = \frac{1}{\rho'_1} \times \left[-\left(y - y_0 - \frac{\delta y}{2}\right)\hat{x} + \left(x - x_0 - \frac{\delta x}{2}\right)\hat{y}\right].$$

Now, we use equations (33) and (5) to calculate the reciprocal vector of the resulting moiré pattern, in which their centers are separated symmetrically by a distance $(\delta x, \delta y)$. For simplicity we assume that the gratings' constants are identical $(s_1 = s_2 = s)$ and $l_1 \neq l_2$, and the branch points are located at different coordinates such as $\left(x_{0_{1,2}}, y_{0_{1,2}}\right)$. Then, we get:

$$\mathbf{G}_{\text{moiré}} = \frac{2\pi}{s}(\delta x\,\hat{x} + \delta y\,\hat{y}) - \left(\frac{l_1}{\rho'_1}\hat{\varphi}'_1 - \frac{l_2}{\rho'_2}\hat{\varphi}'_2\right), \tag{34}$$

where $\hat{\varphi}'_{1,2}$ are unit vectors of azimuthal coordinates $\varphi'_{1,2}$, defined at the centers of branch points located at $\left(x_{0_{1,2}} \mp \frac{\delta x}{2}, y_{0_{1,2}} \mp \frac{\delta y}{2}\right)$ and $\rho'_{1,2}$ are radial coordinates measured from the branch points, respectively. The first term in the last equation shows that the produced moiré pattern has linear shape with a constant period of $\Lambda = s\Big/\left(\delta x^2 + \delta y^2\right)^{1/2}$. The moiré fringes' orientation is perpendicular to the line connecting the origins of the gratings and moiré fringes will have an angle of $\gamma = \tan^{-1}(-\delta x/\delta y)$ with the x-axis. Second term in equation (34) indicates that two fork-shaped patterns will appear in the resulting moiré pattern, in which their branch points located at $\left(x_{0_{1,2}} \mp \frac{\delta x}{2}, y_{0_{1,2}} \mp \frac{\delta y}{2}\right)$, respectively. The defect numbers are equal to the absolute value of the defect numbers of the corresponding gratings.

Finally, we consider a case in which the, direction of the vector connecting the center of first grating to the center of the second one lies in the $+\hat{x}$ direction. As illustrated in figure 9, in this case, branching direction of the generated fork-shaped moiré pattern at the vicinity of the first grating's branch point follows the sign of $+l_1$ and the other shape follows the $-l_2$ sign (see equation (12) and figure 1).

7. Moiré patterns of an LFG and a DZP

In this section, formulation of moiré pattern of superimposition of an LFG and a DZP is presented. We assume that the defect number and grating constant of DZP are l_1 and s, respectively, and the defect number and period of LFG are l_2 and Λ, respectively. In addition, we assume that the centers

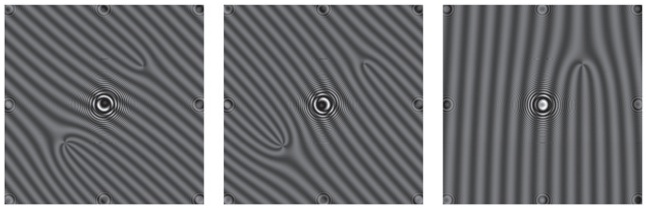

Figure 9. Moiré patterns of two DZPs, in a case, their centers not coincident. Both of the gratings' constants are identical, $s = 0.006\ \text{cm}^2$, and defect numbers are $l_1 = 2$ and $l_2 = 5$. The centers of the gratings separated by (a) $(\delta x, \delta y) = (0.03, 0.03)$ cm, (b) $(\delta x, \delta y) = (-0.03, -0.03)$cm and (c) $(\delta x, \delta y) = (0.03, 0)$cm. In (a) and (b) the branch points coordinates are $(x_{0_1}, y_{0_1}) = (0.5, 0.5)$ and $(x_{0_2}, y_{0_2}) = (-0.5, -0.5)$, respectively. In (c) $(x_{0_1}, y_{0_1}) = (0.515, 0.5)$ and $(x_{0_2}, y_{0_2}) = (0.485, 0.5)$ in which two branch points coincident after displacement.

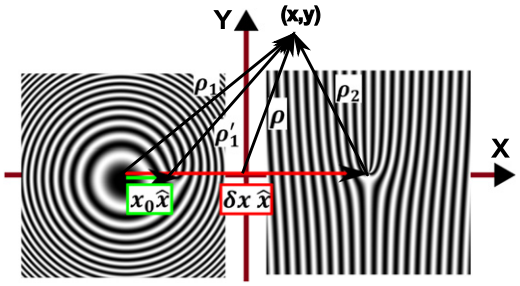

Figure 10. Presentation of different radial vectors in the superimposition of an DZP on an LFG. The values $\boldsymbol{\rho}$, $\boldsymbol{\rho}_1$, $\boldsymbol{\rho}'_1$, and $\boldsymbol{\rho}_2$, are position vectors originated from center of presented Cartesian coordinates system, center and branch point of DZP, and center of LFG to a given point (x, y) in the superimposition area, respectively. $x_0\hat{x}$ is position vector starts from center of DZP and ends at its branch point and $\delta x\hat{x}$ is a vector connecting center of DZP to center of LFG.

of the two gratings separated along the x-direction by a value of δx. We consider that center and branch point of DZP are located at $\left(-\frac{\delta x}{2}, 0\right)$ and $\left(x_0 - \frac{\delta x}{2}, y_0\right)$, respectively. Also, the branch point and center of LFG coincident and located at $\left(\frac{\delta x}{2}, 0\right)$, and lines of LFG are almost in the y-direction. In this section, we use four radial vectors $\boldsymbol{\rho}, \boldsymbol{\rho}_1, \boldsymbol{\rho}'_1$, and $\boldsymbol{\rho}_2$, as illustrated in figure 10. By considering $\alpha = 0$ and using equations (13) and (33), the reciprocal vectors of DZP and LFG are given by:

$$\begin{cases} \mathbf{G}^{\text{DZP}}_{-\delta x/2} &= \dfrac{2\pi}{s}\left[\left(x + \dfrac{\delta x}{2}\right)\hat{x} + y\,\hat{y}\right] - \dfrac{l_1}{\rho'_1}\hat{\varphi}'_1 \\ &= \dfrac{2\pi}{s}\boldsymbol{\rho}_1 - \dfrac{l_1}{\rho'_1}\hat{\varphi}'_1, \\ \mathbf{G}^{\text{LFG}}_{\delta x/2} &= \dfrac{2\pi}{\Lambda}\hat{x} - \dfrac{l_2}{\rho_2}\hat{\varphi}_2, \end{cases} \tag{35}$$

respectively. Considering both sum and difference frequencies in equation (5) leads to:

$$\mathbf{G}_{\text{moiré}} = \frac{2\pi}{s}\left(\boldsymbol{\rho}_1 \mp \frac{s}{\Lambda}\hat{x}\right) \pm \frac{l_2}{\rho_2}\hat{\varphi}_2 - \frac{l_1}{\rho'_1}\hat{\varphi}'_1. \tag{36}$$

As period of DZP is varying as a function of the radial coordinate (see equation (26)) and LFG has a constant period, for the case of $\sqrt{s} > \Lambda$, there are two places over the superimposition area, in which their periods are equal. When a branch point of LFG locates on one of these points, we have $\delta x = \pm s/\Lambda$ and as a result the phrase in parenthesis of equation (36) is equal to $\boldsymbol{\rho}_2$ (see figure 10). Then we have:

$$\mathbf{G}_{\text{moiré}} = \frac{2\pi}{s}\boldsymbol{\rho}_2 \pm \frac{l_2}{\rho_2}\hat{\varphi}_2 - \frac{l_1}{\rho'_1}\hat{\varphi}'_1, \tag{37}$$

The first two terms of equation (37) together show a moiré pattern which is a non-magnified SZP with pattern constant and defect number of s and $\mp l_2$, respectively. The minus sign corresponds to a plus value of δx. Minus value of δx indicates a little different case, in which the center of the DZP is placed on the right side of the center of the LFG, and it refers to the plus value of l_2 in this equation.

Now, let us to investigation effect of third term in equation (36). In this regard, we assume that periods of DZP and LFG at the location of branch point of DZP to be equal, and branch point of DZP located on x-axis, then equation (26) leads to $x_0 = \pm s/\Lambda$. Positive value of x_0 corresponds to $+s/\Lambda$ and negative value of it corresponds to $-s/\Lambda$. According to figure 10, the reciprocal vector of the resulting moiré pattern in equation (36) changes as below:

$$\mathbf{G}_{\text{moiré}} = \frac{2\pi}{s}\boldsymbol{\rho}'_1 \pm \frac{l_2}{\rho_2}\hat{\varphi}_2 - \frac{l_1}{\rho'_1}\hat{\varphi}'_1. \tag{38}$$

Again, the first and third terms of equation (38) indicate a non-magnified SZP with a defect number equal to l_1, in which its center located at the branch point of DZP. Here, the second term does not produce an interesting pattern, except when the periods of both gratings are equal in the branch point of the LFG as discussed previously.

As the last case, we consider that branch points of two gratings coincident. Consequently, $\delta x = x_0$ and vectors $\boldsymbol{\rho}'_1$ and $\boldsymbol{\rho}_2$ are equal, and unit vectors $\hat{\varphi}'_1$ and $\hat{\varphi}_2$ are identical. In addition, if the periods of two gratings are equal in common branch point, we get $\delta x = x_0 = \pm s/\Lambda$ and equation (36) leads to:

$$\mathbf{G}_{\text{moiré}} = \frac{2\pi}{s}\boldsymbol{\rho}'_1 - \frac{l_1 \mp l_2}{\rho'_1}\hat{\varphi}'_1, \tag{39}$$

Here, this equation also indicates a non-magnified SZP with center in the common branch point and defect number equal to $(l_1 \mp l_2)$. Minus and plus signs refer to positive and negative values of x_0, respectively. These behaviors are illustrated in figure 11.

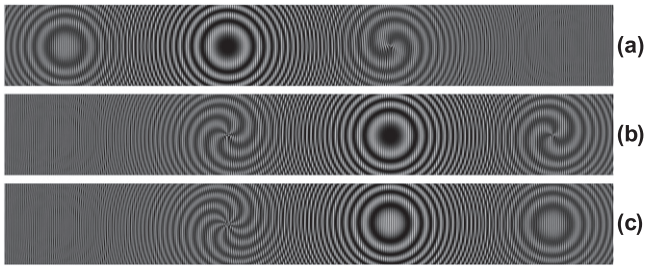

Figure 11. Typical moiré patterns of superimposition of a DZP on an LFG. Defect number and grating constant of DZP are $l_1 = 3$ and $s = 0.05$ cm^2, respectively. For LFG, $l_2 = 5$ and $\Lambda = 0.025$ cm are considered. Mentioned numbers correspond to an area of 7×1 cm^2 for each pattern. In (a) it is assumed that two branch points coincident and for DZP $(x_0, y_0) = (2, 0)$cm and $\delta x = +2$ cm. As a result around the branch point a non-magnified SZP pattern having defect number of $l = l_1 - l_2 = -2$ appeared (see equation (39)). In (b) by considering $\delta x = -2$ cm, around the branch point of LFG (on the left side) a non-magnified SZP having defect number of $l = l_2 = +5$ (see equation (37)) is formed, and in the branch point of the DZP (on the right side) another non-magnified SZP having defect number of $l = l_1 = +3$ is formed (see equation (38)). In (c) by considering $\delta x = -2$ cm and $(x_0, y_0) = (-2, 0)$ cm and that the branch points coincident again (at the left side) a non-magnified SZP pattern having defect number of $l = (l_1 + l_2) = 8$ appeared (see equation (39)).

8. Conclusion

In this work, a very simple, uniform, and comprehensive formulation for the moiré patterns of superimposition of a pair of gratings having topological defects (various superimposition of a pair of LFGs and/or DZPs) based on the reciprocal vectors approach is presented. Phase singularities of the overlaid gratings are considered basically in a simple manner in the presented formulation. For different cases, moiré patterns' formulations are investigated and corresponding simulations presented by MATLAB programming. Results of formulation and simulation are completely confirmed each other. The presented formulation has potential applications in singular optics measurements. As a direct allusion, a grating containing topological defect can be produced when a plane wave interferes with a wave containing phase singularity. Meanwhile, by superpositions of optical fields with the vortices, interference fringes similar to the moiré patterns can be obtained [17, 45]. In addition, it seems that these kinds of moiré patterns in an arrangement of gratings in which they are apart such as in the moiré deflectometry and in the Talbot interferometry may have fantastic applications. Investigation of moiré patterns with the superimposition of two radial or two circular gratings and their mutual superimpositions with each other or with LFGs or DZPs when they are possess branching points with the presented method is very interesting research subject. Results of these kinds of superimpositions are very interesting too, and new aspects of this moiré technique's applications can be found in these kinds of superimpositions. Due to space limitations results of these kinds of superimpositions are not presented in current work. Finally, consideration of the dynamic behavior of these kind moiré patterns when superimposed gratings are moved with respect to each other is another interesting subject.

Acknowledgments

The authors thank the anonymous referees for their constructive comments.

References

[1] Amidror I 2009 *The Theory of the Moiré Phenomenon* vol 1 Periodic Layers (Berlin: Springer) 1
[2] Patorski K and Kujawinska M 1993 *Handbook of the Moiré Fringe Technique* (Amsterdam: Elsevier)
[3] Walker C A 2004 *Handbook of Moiré Measurement* (Bristol: Institute of Physics Publishing)
[4] Indebetouw G and Czarnek R 1992 *Selected Papers on Optical Moiré and Applications* vol 64 (Bellingham, WA: SPIE Optical Engineering Press)
[5] Wen J, Zhang Y and Xiao M 2013 The Talbot effect: recent advances in classical optics, nonlinear optics, and quantum optics *Adv. Opt. Photon.* **5** 83–130
[6] Jamshidi-Ghaleh K and Mansour N 2004 Nonlinear refraction measurements of materials using the moiré deflectometry *Opt. Commun.* **234** 419–25
[7] Rasouli S, Ghasemi H, Tavassoly M and Khalesifard H 2011 Application of 'parallel' moiré deflectometry and the single beam Z-scan technique in the measurement of the nonlinear refractive index *Appl. Opt.* **50** 2356–60
[8] Rasouli S and Tavassoly M T 2006 Application of moiré technique to the measurement of the atmospheric turbulence parameters related to the angle of arrival fluctuations *Opt. Lett.* **31** 3276–8
[9] Rasouli S and Tavassoly M T 2006 Measurement of the refractive-index structure constant, Cn2, and its profile in the ground level atmosphere by moiré technique *Proc. SPIE* **6364** 63640G
[10] Rasouli S and Tavassoly M T 2008 Application of the moiré deflectometry on divergent laser beam to the measurement of the angle of arrival fluctuations and the refractive index structure constant in the turbulent atmosphere *Opt. Lett.* **33** 980–2
[11] Rasouli S 2010 Use of a moiré deflectometer on a telescope for atmospheric turbulence measurements *Opt. Lett.* **35** 1470–2
[12] Rasouli S, Ramaprakash A N, Das H K, Rajarshi C V, Rajabi Y and Dashti M 2009 Two-channel wavefront sensor arrangement employing moiré deflectometry *Proc. SPIE* **7476** 74760K
[13] Dashti M and Rasouli S 2012 Measurement and statistical analysis of the wavefront distortions induced by atmospheric turbulence using two-channel moiré deflectometry *J. Opt.* **14** 095704
[14] Rasouli S, Dashti M and Ramaprakash A N 2010 An adjustable, high sensitivity, wide dynamic range two channel wave-front sensor based on moiré deflectometry *Opt. Express* **18** 23906–15
[15] Yeganeh M, Rasouli S, Dashti M, Slussarenko S, Santamato E and Karimi E 2013 Reconstructing the Poynting vector skew angle and wavefront of optical vortex beams via two-channel moiré deflectometery *Opt. Lett.* **38** 887–9
[16] Yeganeh M and Rasouli S 2013 Use of a two-channel moiré wavefront sensor for measuring topological charge

sign of the vortex beam and investigation of its change due to an odd number of reflections *Int. J. Opt. Photon.* **7** 77–84
[17] Huguenin J A O, Almeida M P, Ribeiro P H S and Khoury A Z 2005 Moiré fringe patterns in spatial quantum correlations of twin photons *Phys. Rev.* A **71** 043818–1-4
[18] Almeida M P, Huguenin J A O, Souto Ribeiro P H and Khoury A Z 2006 Theoretical investigation of moiré patterns in quantum images *J. Mod. Opt.* **53** 777–85
[19] Nishijima Y and Oster G 1964 Moiré Patterns: their application to refractive index and refractiveindex gradient measurements *J. Opt. Soc. Am.* **54** 1–4
[20] Oster G, Wasserman M and Zwerling C 1964 Theoretical interpretation of moiré patterns *J. Opt. Soc. Am.* **54** 169–75
[21] Bryngdahl O 1974 Moiré: formation and interpretation *J. Opt. Soc. Am.* **64** 1287–94
[22] Bryngdahl O 1975 Moiré and higher grating harmonics *J. Opt. Soc. Am.* **65** 685–94
[23] Rogers G 1959 A simple method of calculating moiré patterns *Proc. Phys. Soc.* **73** 142
[24] Rogers G 1977 A geometrical approach to moiré pattern calculations *J. Mod. Opt.* **24** 1–13
[25] Amidror I 2007 *The Theory of the Moiré Phenomenon* vol 2 Aperiodic Layers (Berlin: Springer)
[26] Abolhassani M 2011 Formulation of moiré fringes based on spatial averaging *Optik* **122** 510–3
[27] Kong L, Cai S, Li Z, Jin G, Huang S, Xu K and Wang T 2011 Interpretation of moiré phenomenon in the image domain *Opt. Express* **19** 18399–409
[28] Jaroszewicz Z 1992 A review of Fresnel zone plate moiré patterns obtained by translations *Opt. Eng., Bellingham* **31** 458–64
[29] Lee W and Yuan X 2004 Experimental observation of'pure helical phase' interference using moiré fringes generated from holograms with dislocations *J. Opt. A: Pure Appl. Opt.* **6** 482–85
[30] Zhang P, Huang S, Hu Y, Hernandez D and Chen Z 2010 Generation and nonlinear self-trapping of optical propelling beams *Opt. Lett.* **35** 3129–31
[31] Zhang P, Zhang Z, Prakash J, Huang S, Hernandez D, Salazar M, Christodoulides D N and Chen Z 2011 Trapping and transporting aerosols with a single optical bottle beam generated by moiré techniques *Opt. Lett.* **36** 1491–3
[32] Zhang P, Hernandez D, Cannan D, Hu Y, Fardad S, Huang S, Chen J C, Christodoulides D N and Chen Z 2012 Trapping and rotating microparticles and bacteria with moiré-based optical propelling beams *Biomed. Opt. Express* **3** 1891–7
[33] Senthilkumaran P 2003 Optical phase singularities in detection of laser beam collimation *Appl. Opt.* **42** 6314–20
[34] Chang C-W and Su D-C 1991 Collimation method that uses spiral gratings and Talbot interferometry *Opt. Lett.* **16** 1783–4
[35] Huguenin J A O, Santos B C D, Santos P A M and Khoury A Z 2003 Topological defects in moiré fringes with spiral zone plates *J. Opt. Soc. Am.* A **20** 1883–9
[36] Tavassoly M T and Samavati K 2014 Formulation of the moiré fringes formed by superimposing linear gratings with slowly varying parameters *Appl. Opt.* **53** 6612–8
[37] MacDonald A H and Bistritzer R 2011 Materials science: graphene moiré mystery solved? *Nature* **474** 453–4
[38] Rasouli S and Tavassoly M T 2012 Analysis of the moiré pattern of moving periodic structures using reciprocal vector approach *J. Phys. Conf. Ser.* **350** 012032
[39] Heckenberg N, McDuff R, Smith C and White A 1992 Generation of optical phase singularities by computer-generated holograms *Opt. Lett.* **17** 221–3
[40] Arlt J, Dholakia K, Allen L and Padgett M 1998 The production of multiringed Laguerre–Gaussian modes by computer-generated holograms *J. Mod. Opt.* **45** 1231–7
[41] Janicijevic L and Topuzoski S 2008 Fresnel and Fraunhofer diffraction of a Gaussian laser beam by fork-shaped gratings *J. Opt. Soc. Am.* A **25** 2659–69
[42] Heckenberg N R, McDuff R, Smith C P, Rubinsztein-Dunlop H and Wegener M J 1992 Laser beams with phase singularities *Opt. Quantum Electron.* **24** S951–2
[43] Bass M, Enoch J M, Stryland E W V and Wolfe W L 2000 *Handbook of Optics* 3 (New York: McGraw-Hill) 23.1-23.3
[44] Sharma M K, Singh R K, Joseph J and Senthilkumaran P 2013 Fourier spectrum analysis of spiral zone plates *Opt. Commun.* **304** 43–8
[45] Senthilkumaran P, Masajada J and Shunichi S 2012 Interferometry with vortices *Int. J. Opt.* **2012** 517591